

# Journal of Materials Chemistry A

Accepted Manuscript



This is an *Accepted Manuscript*, which has been through the Royal Society of Chemistry peer review process and has been accepted for publication.

*Accepted Manuscripts* are published online shortly after acceptance, before technical editing, formatting and proof reading. Using this free service, authors can make their results available to the community, in citable form, before we publish the edited article. We will replace this *Accepted Manuscript* with the edited and formatted *Advance Article* as soon as it is available.

You can find more information about *Accepted Manuscripts* in the [Information for Authors](#).

Please note that technical editing may introduce minor changes to the text and/or graphics, which may alter content. The journal's standard [Terms & Conditions](#) and the [Ethical guidelines](#) still apply. In no event shall the Royal Society of Chemistry be held responsible for any errors or omissions in this *Accepted Manuscript* or any consequences arising from the use of any information it contains.

# Sulfur loaded in curved graphene and coated with conductive polyaniline: Preparation and performance as cathode of lithium-sulfur battery

Xiaogang Li<sup>a, b</sup>, Mumin Rao<sup>c</sup>, Haibin Lin<sup>a</sup>, Dongrui Chen<sup>a</sup>, Yanlin Liu<sup>a</sup>, Shizhu Liu<sup>a</sup>,  
Youhao Liao<sup>a, c</sup>, Lidan Xing<sup>a, c</sup>, Mengqing Xu<sup>a, c</sup>, Weishan Li<sup>a, b, c, \*</sup>

<sup>a</sup> School of Chemistry and Environment, South China Normal University, Guangzhou 510006, China

<sup>b</sup> College of Materials Science and Engineering, South China University of Technology, Guangzhou 510641, China

<sup>c</sup> Engineering Research Center of MTEES (Ministry of Education), Research Center of BMET (Guangdong Province), Engineering Lab. of OFMHEB (Guangdong Province), Key Lab. of ETESPG (GHEI), and Innovative Platform for ITBMD (Guangzhou Municipality), South China Normal University, Guangzhou 510006, China

## Abstract

We report a composite (CG-S@PANI), sulfur (S) loaded in curved graphene (CG) and coated with conductive polyaniline (PANI), as cathode of lithium-sulfur battery. CG is prepared by splitting multi-wall carbon nanotubes and loaded with S via

---

\* Corresponding author: School of Chemistry and Environment, South China Normal University. E-mail address: liwsh@scnu.edu.cn (W. S. Li).

chemical deposition and then coated with polyaniline *via in situ* polymerization under the control of ascorbic acid. The physical and electrochemical performances of the resulting CG-S@PANI are investigated by nitrogen adsorption-desorption isotherms, X-ray powder diffraction, thermogravimetric analysis, transmission electron microscopy, electrochemical impedance spectroscopy, charge-discharge test, and electronic conductivity measurement. CG-S@PANI as cathode of lithium-sulfur battery delivers an initial discharge capacity of 851 mAh·g<sup>-1</sup> (616 mAh·g<sup>-1</sup> on the base of cathode mass) at 0.2 C with a capacity retention of over 90% after 100 cycles. This nature is attributed to the co-contribution of CG and conductive PANI to the concurrent improvement in electronic conductivity and chemical stability of sulfur cathode.

## 1. Introduction

Sulfur as cathode of lithium battery has attracted much attention, due to its high theoretical gravimetric energy density (2600 Wh·kg<sup>-1</sup>) and volumetric energy density (2800 Wh·L<sup>-1</sup>), abundance on earth, and environmental benignity.<sup>1-8</sup> However, there are still issues that restrict its commercial application in lithium battery.<sup>1,9-11</sup> Firstly, sulfur and its discharge products, lithium disulfide and lithium sulfide (Li<sub>2</sub>S<sub>2</sub>/Li<sub>2</sub>S), are electronic and ionic insulators, leading to the severe polarization during charge-discharge process. Secondly, the intermediates, lithium polysulfides (Li<sub>2</sub>S<sub>x</sub>, 2<x≤8), are highly soluble in the organic electrolyte, resulting in the so-called shuttle effect and decreasing the coulombic efficiency of the lithium sulfur battery. Thirdly,

there is a significant volume change, as large as 80% during charge-discharge process, giving rise to the pulverization and destruction of the cathode. These problems result in the poor cyclic stability and rate capability of lithium-sulfur battery.

Many approaches have been attempted to solve these problems. Among these approaches, the introduction of nanostructured carbon materials into sulfur cathode is found to be effective for improving comprehensive performances of sulfur cathode. Several nano-carbon materials have been reported as the matrix of sulfur including carbon nanotube,<sup>12-21</sup> carbon nanofiber,<sup>22-24</sup> mesoporous carbon,<sup>25-27</sup> graphene,<sup>28-33</sup> and hollow carbon spheres.<sup>34-35</sup>

Compared with other spherical and planar materials, carbon nanotubes (CNTs) exhibit unique advantages, including well-defined nanostructure, highly electronic conductivity, strong rigidity, and chemical stability. However, typical CNTs are prepared with lengths in the range of micrometers and are aggregated into macroscopically entangled ropes or masses, which do not facilitate the loading of sulfur in cathode and yield low specific energy density of lithium-sulfur battery. Graphene is a two-dimensional monolayer of  $sp^2$ -hybridized carbon atoms with a honeycomb lattice structure, possessing unusual mechanical strength, excellent electrical conductivity and good thermal stability.<sup>28-33</sup> Graphene is usually flat, however, which does not facilitate the loading of sulfur.

In the applications of nano-carbon materials in sulfur cathode, the direct contact of sulfur with electrolyte is inevitable and the dissolution and diffusion of intermediate lithium polysulfides still exist in lithium-sulfur battery. To solve this problem,

conductive polymers such as polyaniline and polypyrrole have been used to coat the sulfur composites.<sup>36-39</sup> Besides their electronic conductivity, conductive polymers exhibit abundantly porous structure and insolubility in organic electrolytes and thus are suitable for the application in batteries based on organic electrolytes. Furthermore, the conductive polyaniline synthesized under the control of ascorbic acid lowers the toxicity and improves the electronic conductivity.<sup>40-44</sup>

In this work, we proposed a novel composite, sulfur loaded in curved graphene and coated with conductive polyaniline, as cathode of lithium-sulfur battery. As shown in Fig. 1, the curved graphene was prepared by splitting multi-wall carbon nanotubes in transversal and longitudinal directions. Compared with flat graphene, the curved structure of the curved graphene provides the space for loading more sulfur. Polyaniline was coated on the curved graphene loaded with sulfur *via in situ* polymerization under the control of ascorbic acid, which avoids the direct contact between sulfur and electrolyte. This configuration is expected to be beneficial for the improvement of cyclic stability and rate capability.

## 2. Experimental

### 2.1 Preparation of curved graphene

Raw multi-walled carbon nanotubes (MWCNTs) are layered graphene that is rolled up into seamless tubes. As a result, it is possible to obtain curved graphene (CG) by longitudinally unzipping carbon nanotubes in highly oxidizing solutions.<sup>45-51</sup>

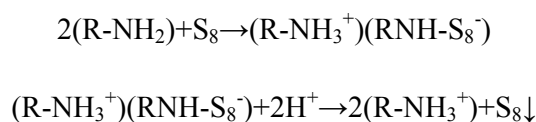
In a typical procedure, MWCNTs (provided by CNano Technology Limited, 150

mg) were suspended in concentrated  $\text{H}_2\text{SO}_4$  (98%, 36 mL) under stirring for 1 h. Concentrated  $\text{H}_3\text{PO}_4$  (85%, 4 mL) was then added under stirring for 30 min.  $\text{KMnO}_4$  (750 mg) was then slowly added under stirring for 1 h at room temperature. The resulting slurry was heated at 65 °C for 2 h and then 100 mL of ice with  $\text{H}_2\text{O}_2$  (30%, 5 mL) was added to prevent the precipitation of insoluble  $\text{MnO}_2$ . The product was allowed to coagulate (no stirring) for 24 h. The top portion was decanted from the solid, and the remaining portion was filtered over a 200 nm pore size PTFE membrane. The brown filter cake was washed twice with 20% HCl (6 mL each), resuspended in  $\text{H}_2\text{O}$  (60 mL) by stirring for 2 h, and re-coagulated with HCl (30%, 40 mL). The product was filtered on the same PTFE membrane and then dispersed in ethanol (100%, 40 mL) under stirring for 2 h. Ether (60 mL) was then added to the suspension, and the mixture was allowed to coagulate for 1 h before filtering through the same PTFE membrane. The remaining solid was washed twice with ether (10 mL each) and vacuum-dried to yield 260 mg of CG.

## 2.2 Preparation of CG-S@PANI

Specially, 0.5 g prepared CG was firstly suspended in 100 ml diluted hydrochloric acid (HCl, 2 mol/L), and then sonicated at 50 °C for 8 h to obtain a homogeneous dispersion. 5 mL cetyl trimethyl ammonium bromide solution (CTAB, 5 wt%) was successively added into the dispersion under vigorous magnetic stirring. Simultaneously, 2.83 g sublimed sulfur was dissolved in ethylenediamine (EDA) to form an S-EDA precursor solution. The precursor solution was then slowly added to

the CG dispersion in diluted hydrochloric acid. The S-EDA decomposed in the diluted hydrochloric acid and sulfur was loaded in CG through reactions:<sup>52</sup>



The resulting mixture was filtered and dried to obtain CG-S and treated as follows to obtain CG-S@PANI. Moderate amount of 2 mol/L HCl solution was added into the mixture to adjust the pH value to 2.0~3.0. 1.05 g aniline monomer ( $\text{C}_6\text{H}_5\text{NH}_2$ ) and 0.142 g ascorbic acid ( $\text{C}_6\text{H}_8\text{O}_6$ ) were successively added into the mixture under vigorous stirring in ice bath at 15 °C. Meanwhile, 1.838 g ammonium persulphate ( $(\text{NH}_4)_2\text{S}_2\text{O}_8$ ) dissolved in 2 mol/L HCl solution as oxidizer was added dropwise with a speed of about 0.5 mL/min. Ascorbic acid was used as dopant and inhibitor for the formation of bulk polymer resulting from the strong oxidability of ammonium persulphate. The former provides the polymer with electronic conductivity, while the latter, via the reductivity of ascorbic acid, prevents bulk polymerization resulting from the strong oxidability of ammonium persulphate.<sup>53</sup> Under vigorous stirring for 8 h, CG-S@PANI was obtained by rinsing and filtering with diluted HCl, alcohol and deionized water successively, and drying at 60 °C for 24 h.

### 2.3 Coin cell assembling and electrochemical measurements

The cathode was prepared by mixing the synthesized materials, acetylene black (AB) and polyvinylidene difluoride (PVDF) in a weight ratio of 80:10:10 with N-methyl pyrrolidone (NMP) as a dispersant. After mixing, the slurry was coated on

aluminum foil current collector and dried in a vacuum oven at 60 °C for 24 h. The loading mass of sulfur in cathode was about 0.6~1.2 mg/cm<sup>2</sup>. The electrochemical performances were evaluated in CR2025-type coin cells, using lithium metal foil as the counter electrode, polypropylene membrane (Cellgard 2400) as the separator and 1.0 M LiN(CF<sub>3</sub>SO<sub>2</sub>)<sub>2</sub> (LiTFSI, 99%, Aladdin) and 0.1 M lithium nitrate (LiNO<sub>3</sub>, 99%, Aladdin) dissolved in the mixture of ethylene glycol dimethyl ether (EGDME, 99.5%, Aladdin) and 1,3-dioxolane (DOL, 99.5%, Aladdin) (1:1, V/V) as the electrolyte. All the chemicals were used without further treatment. The preparation of the electrolyte and the cell assembly were carried out in an argon-filled glove box with both moisture and oxygen contents less than 1 ppm. The water content in the resulting electrolyte was measured with 831 KF Coulometer (METROHM Ltd. CH-9101 Herisau, Switzerland). It was less than 100 ppm.

The coin cells were galvanostatically discharged and charged using a LAND cell test system (Land CT 2001A, China) between 1.5-2.8 V vs Li<sup>+</sup>/Li<sup>0</sup>. Electrochemical impedance measurements were performed at the fully charged state of the sulfur electrode on AUTOLAB PGSTAT302 (The Netherlands) from 100 kHz to 0.01 Hz at an amplitude of 5 mV. The specific capacity was reported based on the mass of element sulfur except for special remark. All electrochemical measurements were carried out at room temperature.

## 2.4 Physical characterizations

The morphology of samples was observed using high-resolution transmission

electron microscopy (HRTEM, JEM-2100HP) at 100~200 kV. The sulfur content of the prepared composite was determined by thermogravimetric analysis (Perkin-Elmer TGA 7) under N<sub>2</sub> atmosphere from room temperature to 500 °C at a heating rate of 10 °C/min. N<sub>2</sub> adsorption-desorption isotherm measurements were performed with ASAP2020 (Micromeritics, USA) to obtain the BET (Brunauer-Emmett-Teller) specific surface area, BJH (Barrett-Joyner-Halenda) pore size distribution and total pore volume at liquid nitrogen temperature (77 K). The crystal structure was determined with X-ray powder diffraction on BRUKER D8 ADVANCE in the Bragg's angle ( $2\theta$ ) range from 10° to 80° with monochromatic Cu K $\alpha$  radiation. The electronic conductivity of the composites was measured on a four point probe double electric logging tester (RTS-9 type, Guangzhou Four-point Probe Technology Co., LTD) at room temperature. The composite film for conductivity measurement was prepared by pressing the composite of 100 mg into a disc with 12 mm in diameter and 0.5~1.0  $\mu$ m thick under a pressure of 12 MPa for 5 seconds.

### 3. Results and discussion

The morphology of the samples was observed using TEM, the obtained results are presented in Fig. 2. The tubular morphology and the layered structure can be clearly identified, as shown in Fig. 2a. After longitudinally cutting and unzipping raw MWCNTs using Hummers method,<sup>45-51</sup> the carbon tubes were split into pieces with curved shape and layered structure, as shown in Fig. 2b. We label this material as curved graphene (CG). This cutting procedure facilitates the formation of

oxygen-containing functionalities such as carbonyls, carboxyls and hydroxyls, which is beneficial for loading sulfur.<sup>45-46</sup> Based on the different images between Fig. 2b and c, it can be inferred that sulfur have been filled in the CG. We label this product as CG-S. When CG-S is treated in aniline-containing solution, its diameter increases, as shown in Fig. 2d, indicating that polyaniline has been successfully coated on CG-S. We label this product as CG-S@PANI. The coated polyaniline confines the sulfur and provides electronically conductive network, which should contributes to the cyclic stability and rate capability of sulfur cathode.

X-ray diffraction characterization was performed to identify the structure of sulfur existing in the resulting product. Fig. 3 presents the X-ray diffraction patterns of sublimed sulfur, raw MWCNTs, CG, PANI, CG-S, and CG-S@PANI. Raw MWCNTs and CG show the similar amorphous carbon state with two wide peaks centered at  $2\theta = 26.4^\circ$  and  $43^\circ$  in the XRD pattern, indicating that the cutting of MWCNTs does not change its layered structure. PANI also demonstrate amorphous state with two wide peaks centered at  $2\theta = 20^\circ$  and  $26^\circ$  in the XRD pattern. CG-S and CG-S@PANI have their diffraction similar to sublimed sulfur with sharp diffraction peaks centered at  $2\theta = 23.4^\circ$  and  $28.0^\circ$ , which matches well with the standard card of orthorhombic phase sulfur (JCPDS No. 08-0247).<sup>54</sup> Therefore, the sulfur in CG-S and CG-S@PANI exhibits orthorhombic phase crystal structure of sublimed sulfur, which is the most stable chemically and thermally among all the crystal configurations of sulfur. A larger version of XRD patterns with log (Intensity) is presented in Fig. S1, which confirms that sulfur has been successfully loaded into the CG and suggests that the

resulting samples do not contain any crystalline impurities.

The sulfur content of the as-prepared samples was determined by TGA. Fig. 4 shows the TGA curves of sublimed sulfur, raw MWCNTs, CG, CG-S, and CG-S@PANI, obtained under N<sub>2</sub> atmosphere from room temperature to 500 °C at a heat rate of 10 °C/min. There are about 5% and 28% mass loss for raw MWCNTs and CG, respectively, which is probably ascribed to absorbed moisture below 100 °C and thermal decomposition of oxygen-containing functional groups.<sup>48</sup> It can be seen that the sulfur evaporation happens from about 150 °C to 280 °C.<sup>55</sup> The sulfur content is 85% in CG-S and 55% in CG-S@PANI. It can be noted from Fig. 4 that the release temperature of sulfur in CG-S is slightly lower than simple sublimed sulfur. This phenomenon can be ascribed to the highly dispersed sulfur in CG-S compared to the bulky one in sublimed sulfur. CG-S@PANI shows additional weight loss at the temperature lower than 150 °C compared to CG-S, which should be related to the release of volatile compositions in PANI, including adsorbed water from air and the decomposition products of PANI. The sulfur release in CG-S@PANI behave similar to that in CG-S due to the PANI decomposition, while the residue from PANI decomposition yields a resistance to the further release of sulfur, leading to different change of CG-S@PANI from sublimed sulfur and CG-S at the temperature from ~200 °C to 275°C.

The N<sub>2</sub> adsorption-desorption isotherm measurements were performed to understand the pore structure of the resulting products. Fig. 5 presents the sorption isotherms and DFT pore size distribution curves of CG, CG-S and CG-S@PANI. It

can be seen that all samples possess a typical IV-type isotherm, which corresponds to a small mesoporous structure (Fig. 5 inset). The obtained BET specific surface area is 24.1, 4.5 and 20.9  $\text{m}^2\cdot\text{g}^{-1}$  for CG, CG-S and CG-S@PANI, corresponding to total pore volume of 0.061, 0.018 and 0.066  $\text{cm}^3\cdot\text{g}^{-1}$ , respectively. These results demonstrate that the sulfur has been successfully loaded and the coated PANI is porous, which is beneficial for lithium ion transportation.

Coin cells were setup to evaluate the electrochemical performances of the resulting products. Fig. 6 presents the selected charge-discharge profiles of CG-S and CG-S@PANI at 0.02 C (1 C = 1672  $\text{mA}\cdot\text{g}^{-1}$ ) for the first three cycles and at 0.2 C for the subsequent cycles, which are characteristic of sulfur cathode. The first charge-discharge cycle is performed at 0.02 C for activation, in which both CG-S (Fig. 6a) and CG-S@PANI (Fig. 6b) show two discharge plateaus at around 2.3 V and 2.1 V, corresponding to the reductions of element sulfur to high order polysulfides such as  $\text{Li}_2\text{S}_8$  and then to  $\text{Li}_2\text{S}$  or  $\text{Li}_2\text{S}_2$ , while the long charge plateau corresponds to the oxidation of  $\text{Li}_2\text{S}$  or  $\text{Li}_2\text{S}_2$  and long-chain polysulfides. The abrupt voltage rise at the beginning of charge stage is ascribed to the serious polarization of electrode, which results from the slow kinetics for the oxidation of  $\text{Li}_2\text{S}_2$  and  $\text{Li}_2\text{S}$  to soluble long-chain polysulfides. CG-S@PANI delivers a higher initial specific discharge capacity (1300.1  $\text{mAh}\cdot\text{g}^{-1}$ , 818.4  $\text{mAh}\cdot\text{g}^{-1}$  on base of the cathode mass) than CG-S (1029.6  $\text{mAh}\cdot\text{g}^{-1}$ , 673.5  $\text{mAh}\cdot\text{g}^{-1}$  on base of the cathode mass) at 0.02 C rate, showing that the sulfur in CG-S@PANI is exploited more efficiently than that in CG-S, which can be ascribed to the improved electronic conductivity of the cathode by PANI. It can be

seen from Fig. 6 that there is a larger polarization for CG-S@PANI than CG-S during charging and discharging processes. This polarization can be ascribed to PANI coating, which reduces lithium transportation.

When the cells are cycled at 0.2 C, the discharge capacity decreases significantly for CG-S but maintains a high level for CG-S@PANI. Fig. 7 compares the cyclic stability of CG-S and CG-S@PANI at 0.2 C. CG-S@PANI delivers an initial discharge capacity of  $851 \text{ mAh}\cdot\text{g}^{-1}$  ( $378.2 \text{ mAh}\cdot\text{g}^{-1}$  on base of the cathode mass) at 0.2 C and remains  $633.1 \text{ mAh}\cdot\text{g}^{-1}$  ( $281.4 \text{ mAh}\cdot\text{g}^{-1}$  on base of the cathode mass) with a capacity retention of 90.1% after 100 cycles. However, CG-S delivers an initial discharge capacity of  $616.2 \text{ mAh}\cdot\text{g}^{-1}$  ( $425 \text{ mAh}\cdot\text{g}^{-1}$  on base of the cathode mass) at 0.2 C and remains  $166.1 \text{ mAh}\cdot\text{g}^{-1}$  ( $114.6 \text{ mAh}\cdot\text{g}^{-1}$  on base of the cathode mass) with a capacity retention of 30% after 100 cycles. This result indicates that the sulfur in CG-S@PANI is more stable chemically than that in CG-S. The improved stability of sulfur in CG-S@PANI should be ascribed to the confining of sulfur by PANI, which suppresses the dissolution of intermediates from sulfur reduction. The higher coulombic efficiency of CG-S@PANI (98%) than CG-S (81%) confirms this suppression.

Fig. 8 presented cyclic performances of two cathodes under various current rates. It can be seen from Fig. 8 that CG-S@PANI exhibits far better rate capability than CG-S. For example, the average specific capacity is  $615.8 \text{ mAh}\cdot\text{g}^{-1}$  ( $493 \text{ mAh}\cdot\text{g}^{-1}$  on base of the cathode mass) for CG-S@PANI at 0.2 C, but only  $333.5 \text{ mAh}\cdot\text{g}^{-1}$  ( $267 \text{ mAh}\cdot\text{g}^{-1}$  on base of the cathode mass) for CG-S. Importantly, after rate capability test,

CG-S@PANI recovers its average discharge capacity to  $931.2 \text{ mAh}\cdot\text{g}^{-1}$  ( $745 \text{ mAh}\cdot\text{g}^{-1}$  on base of the cathode mass) at  $0.05 \text{ C}$ , compared to CG-S with the discharge capacity dropped significantly to  $324.1 \text{ mAh}\cdot\text{g}^{-1}$  ( $260 \text{ mAh}\cdot\text{g}^{-1}$  on base of the cathode mass). Apparently, PANI contributes to not only the cyclic stability but also the rate capability of sulfur cathode. The improved rate capability should be related to the electronic conductivity of PANI, which can be confirmed by four point probe test. The obtained electronic conductivity is  $9.39 \times 10^{-4} \text{ S/cm}$  for CG-S and  $1.04 \text{ S/cm}$  for CG-S@PANI, indicative of the significantly increased electronic conductivity of CG-S by coating PANI. Fig. S2 shows the electrochemical impedance spectra of CG-S and CG-S@PANI at fully charged state after 100 cycles at  $0.2 \text{ C}$ . The spectra of both samples are similar, consisting of the semicircle at high frequency, which reflects the impedance of electrode/electrolyte interface, and the slope line at low frequency, which reflects Warburg diffusion impedance.<sup>56-59</sup> The interfacial resistance, the diameter of the semicircle, reflects the stability of the sulfur electrode, which is  $36.7 \text{ }\Omega$  for CG-S@PANI and  $193 \text{ }\Omega$  for CG-S, indicative of the improved interfacial stability of CG-S by coating PANI. The PANI coating not only provides an electronic conductive network, which contributes to the improved rate capability of the cathode, but also suppresses the dissolution of intermediates, which contributes to the improved cyclic stability of the cathode.

The self-discharge usually takes place in lithium-sulfur battery due to the dissolution and diffusion of soluble polysulfides,<sup>44</sup> and therefore PANI coating not only improves cyclic stability and rate capability of the sulfur cathode but also

protects the cathode from self-discharge. Self-discharge test was performed to identify the contribution of PANI in CG-S@PANI. Fig. 9 presents the voltage variations of the Li/CG-S and Li/CG-S@PANI cells after three discharge/charge cycles at 0.1 C. It can be seen from Fig. 9 that the Li/CG-S cell experiences a serious self-discharge: the cell voltage drops quickly initially, remains stable for a certain time and then drops slowly up to 2.25 V. This phenomenon can be ascribed to the shuttle effect of the intermediates, lithium polysulfides formed during discharge/charge cycle. Lithium polysulfides are reduced on lithium anode and oxidized on sulfur cathode, which is accompanied with the subsequent reduction of sulfur, leading to the voltage drops. The Li/CG-S@PANI cell shows a similar voltage drop initially, which can be ascribed to the self-discharge of the naked sulfur in CG-S@PANI. PANI is used to coat sulfur but part of sulfur in CG-S@PANI is left inevitably exposed to the electrolyte and suffers self-discharge. Differently from Li/CG-S cell, however, the Li/CG-S@PANI cell recovers its voltage at the latter stage, suggesting that the sulfur covered by PANI in CG-S@PANI can be protected from self-discharge.

#### 4. Conclusions

A composite CG-S@PANI has been successfully prepared by loading sulfur on curved graphene (CG) via chemical deposition and further coating conductive polyaniline (PANI) *via in situ* polymerization under the control of ascorbic acid. The performances of the composite as cathode of lithium-sulfur battery were evaluated with physical and electrochemical characterizations. The curved morphology of CG

facilitates the loading of sulfur, the coated PANI provides a protection for the sulfur from dissolution, and the combination of CG and PANI provides electronically conductive framework, leading to the improved cyclic stability and rate capability of the sulfur cathode.

### Acknowledgements

The authors are highly grateful for the financial support from the joint project of National Natural Science Foundation of China and Natural Science Foundation of Guangdong Province (Grant No. U1401248), Natural Science Foundation of Guangdong Province (Grant No. S2013040016471), China Postdoctoral Science Foundation funded project (Grant Nos. 2013M530369 and 2014T70819), the key project of Science and Technology in Guangdong Province (Grant Nos. 2012A090300012 and 2013B090800013), and the scientific research project of Department of Education of Guangdong Province (Grant No. 2013CXZDA013).

### Notes and references

- 1 X. L. Ji, K. T. Lee and L. F. Nazar, *Nat. Mater.*, 2009, **8**, 500.
- 2 M. Winter and R. J. Brod, *Chem. Rev.*, 2004, **104**, 4245.
- 3 P. G. Bruce, *Solid State Ionics*, 2008, **179**, 752.
- 4 Y. Yang, G. Y. Zheng and Y. Cui, *Chem. Soc. Rev.*, 2013, **42**, 3018.
- 5 P. G. Bruce, S. A. Freunberger, L. J. Hardwick and J.-M. Tarascon, *Nat. Mater.*, 2012, **11**, 19.

- 6 M. K. Song, E. J. Cairns, Y. G. Zhang, *Nanoscale*, 2013, **5**, 2186.
- 7 X. L. Ji and L. F. Nazar, *J. Mater. Chem.*, 2010, **20**, 9821.
- 8 Y. V. Mikhaylik and J. R. Akridge, *J. Electrochem. Soc.*, 2004, **151**, A1969.
- 9 Y. Yang, G. Y. Zheng, S. Misra, J. Nelson, M. F. Toney and Y. Gui, *J. Am. Chem. Soc.*, 2012, **134**, 15387.
- 10 R. Elazari, G. Salitra, Y. Talyosef, J. Grinblat, C. Scordilis Kelley, A. Xiao, J. Affinito and D. Aurbach, *J. Electrochem. Soc.*, 2010, **157**, A1131.
- 11 S. Joongpyo, K. A. Striebel and E. J. Cairns, *J. Electrochem. Soc.*, 2002, **149**, A1321.
- 12 X. B. Cheng, H. J. Peng, J. Q. Huang, L. Zhu, S. H. Yang, Y. Liu, H. W. Zhang, W. C. Zhu, F. Wei, Q. Zhang, *J. Power Sources*, 2014, **261**, 264.
- 13 M. Hagen, S. Dörfler, H. Althues, J. Tübke, M. J. Hoffmann, S. Kaskel, K. Pinkwart, *J. Power Sources*, 2012, **213**, 239.
- 14 W. Wei, J. L. Wang, L. J. Zhou, J. Yang, B. Schumann, Y. NuLi, *Electrochem. Commun.*, 2011, **13**, 399.
- 15 L. X. Yuan, H. P. Yuan, X. P. Qiu, L. Q. Chen, W. T. Zhu, *J. Power Sources*, 2009, **189**, 1141.
- 16 H. Kim, J. T. Lee, G. Yushin, *J. Power Sources*, 2013, **226**, 256.
- 17 J. Q. Huang, Q. Zhang, S. M. Zhang, X. F. Liua, W. C. Zhu, W. Z. Qian, F. Wei, *Carbon*, 2013, **58**, 99.
- 18 G. M. Zhou, D. W. Wang, F. Li, P. X. Hou, L. C. Yin, C. Liu, G. Q. (Max) Lu, I. R. Gentle and H. M. Cheng, *Energ. & Environ. Sci.*, 2012, **5**, 8901.

- 19 J. C. Guo, Y. H. Xu, and C. S. Wang, *Nano Lett.*, 2011, **11**, 4288.
- 20 W. Ahn, K. B. Kim, K. N. Jung, K. H. Shin, Ch. S. Jin, *J. Power Sources*, 2012, **202**, 394.
- 21 J. H. Kim, K. Fu, J. Choi, K. Kil, J. Kim, X. G. Han, L. B. Hu & U. Paik, *Sci. Rep.*, 2015, **5**, 8946.
- 22 L. W. Ji, M. M. Rao, S. Aloni, L. Wang, E. J. Cairns and Y. G. Zhang, *Energ. & Environ. Sci.*, 2011, **4**, 5053.
- 23 M. M. Rao, X. Y. Geng, X. P. Li, S. J. Hu, W. S. Li, *J. Power Sources*, 2012, **212**, 179.
- 24 M. M. Rao, X. Y. Song, E. J. Cairns, *J. Power Sources*, 2012, **205**, 474.
- 25 K. A. See, Y. S. Jun, J. A. Gerbec, J. K. Sprafke, F. Wudl, G. D. Stucky, and R. Seshadri, *ACS Appl. Mater. & Inter.*, 2014, **6**, 10908.
- 26 J. Liu, T. Y. Yang, D. W. Wang, G. Q. Lu, D. Y. Zhao & S. Z. Qiao, *Nat. Commun.*, 2014, **4**, 2798.
- 27 T. Xu, J. X. Song, M. L. Gordin, H. Sohn, Z. X. Yu, S. R. Chen, and D. H. Wang, *ACS Appl. Mater. & Inter.*, 2013, **5**, 11355.
- 28 X. Y. Zhou, J. Xie, J. Yang, Y. L. Zou, J. J. Tang, S. C. Wang, L. L. Ma, Q. C. Liao, *J. Power Sources*, 2013, **243**, 993.
- 29 N. W. Li, M. B. Zheng, H. L. Lu, Z. B. Hu, C. F. Shen, X. F. Chang, G. B. Ji, J. M. Cao and Y. Shi, *Chem. Commun.*, 2012, **48**, 4106.
- 30 J. Xie, J. Yang, X. Y. Zhou, Y. L. Zou, J. J. Tang, S. C. Wang, F. Chen, *J. Power Sources*, 2014, **253**, 55.

- 31 M. P. Yu, W. J. Yuan, Ch. Li, J. D. Hong and G. Q. Shi, *J. Mater. Chem. A*, 2014, **2**, 7360.
- 32 G. M. Zhou , S. F. Pei, L. Li, D. W. Wang , S. G. Wang , K. Huang, L. C. Yin , F. Li, and H. M. Cheng, *Adv. Mater.*, 2014, **26**, 625.
- 33 L. W. Ji, M. M. Rao, H. M. Zheng, L. Zhang, Y. C. Li, W. H. Duan, J. H. Guo, E. J. Cairns, and Y. G. Zhang, *J. Am. Chem. Soc.*, 2011, **133**, 18522.
- 34 K. Zhang, Q. Zhao, Z. L. Tao, and J. Chen, *Nano Res.*, 2013, **6**, 38.
- 35 N. Jayaprakash, J. Shen, S. S. Moganty, A. Corona, and L. A. Archer, *Angew. Chem.*, 2011, **123**, 6026.
- 36 L. C. Yin, J. L. Wang, F. J. Lin, J. Yang and Y. Nuli, *Energ. & Environ. Sci.*, 2012, **5**, 6966.
- 37 X. Liang, Z. Y. Wen, Y. Liu, H. Zhang, J. Jin, M. F. Wu, X. W. Wu, *J. Power Sources*, 2012, **206**, 409.
- 38 J. L. Wang, L. C. Yin, H. Jia, H. T. Yu, Y. S. He, J. Yang, and C. W. Monroe, *ChemSusChem*, 2014, **7**, 563.
- 39 Y. G. Zhang, Y. Zhao, T. N. L. Doan, A. Konarov, D. Gosselink, H. G. Soboleski, P. Chen, *Solid State Ionics*, 2013, **238**, 30.
- 40 A. Fedorková, R. Oriňáková, O. Čech, M. Sedlaříková, *Int. J. Electrochem. Sc.*, 2013, **8**, 10308.
- 41 L. Li, G. D. Ruan, Z. W. Peng, Y. Yang, H. L. Fei, A.-R. O. Raji, E. L. G. Samuel, and J. M. Tour, *ACS Appl. Mater. & Inter.*, 2014, **6**, 15033.
- 42 X. G. Li, M. M. Rao, D. R. Chen, H. B. Lin, Y. L. Liu, Y. H. Liao, L. D. Xing, W.

- S. Li, *Electrochim. Acta*, 2015, **166**, 93.
- 43 F. Wu, J. Z. Chen, L. Li, T. Zhao, and R. J. Chen, *J. Phys. Chem. C*, 2011, **115**, 24411.
- 44 H. S. Ryu, H. J. Ahn, K. W. Kim, J. H. Ahn, K. K. Cho, T. H. Nam, *Electrochim. Acta*, 2006, **52**, 1563.
- 45 D. V. Kosynkin, A. L. Higginbotham, A. Sinitskii, J. R. Lomeda, A. Dimiev, B. K. Price1 & J. M. Tour, *Nature*, 2009, **458**, 872.
- 46 A. L. Higginbotham, D. V. Kosynkin, A. Sinitskii, Z. Z. Sun, and J. M. Tour, *ACS NANO*, 2010, **4**, 2059.
- 47 H. W. Wang, Y. L. Wang, Z. G. Hu, and X. F. Wang, *ACS Appl. Mater. & Inter.*, 2012, **4**, 6827.
- 48 B. W. Xiao, X. F. Li, X. Li, B. Q. Wang, C. Langford, R. Y. Li, and X. L. Sun, *J. Phys. Chem. C*, 2014, **118**, 881.
- 49 L. Y. Jiao, L. Zhang, X. R. Wang, G. Diankov & H. J. Dai, *Nature*, 2009, **458** , 877.
- 50 J. L. Li, K. N. Kudin, M. J. McAllister, R. K. Prud'homme, I. A. Aksay, and R. Car, *Phys. Rev. Lett.*, 2006, **96**, 176101.
- 51 T. Saitoa, K. Matsushige, K. Tanaka, *Physica B*, 2002, **323**, 280.
- 52 C. H. Wang , H. W. Chen, W. L. Dong, J. Ge, W. Lu, X. D. Wu, L. Guo and L. W. Chen, *Chem. Commun.*, 2014, **20**, 1202.
- 53 Y. X. Li, W. Y. Li, H. P. Zhou, F. Y. Wang, Y. Chen, Y. Wang, C. Yu, *Sensor Actuat. B: Chem.*, 2015, **208**, 30.

- 54 X. Y. Geng, M. M. Rao, X. P. Li, W. S. Li, *J. Solid State Electr.*, 2013, **17**, 987.
- 55 C. Wang, W. Wan, J. T. Chen, H. H. Zhou, X. X. Zhang, L. X. Yuan and Y. H. Huang, *J. Mater. Chem. A*, 2013, **1**, 1716.
- 56 D. S. Lu, W. S. Li, X. X. Zuo, Z. Z. Yuan, Q. M. Huang, *J. Phys. Chem. C*, 2007, **111**, 12067.
- 57 J. Songa and M. Z. Bazant, *J. Electrochem. Soc.*, 2013, **160**, A15.
- 58 F. Ciucci, W. Lai, *Electrochim. Acta*, 2012, **81**, 205.
- 59 W. Lai, and F. Ciucci, *J. Electrochem. Soc.*, 2011, **158**, A115.

### Figure Captions

**Fig. 1** Schematic configuration of CG-S@PANI composite as cathode of lithium sulfur battery.

**Fig. 2** TEM images of raw MWCNTs (a), CG (b), CG-S (c), and CG-S@PANI (d).

**Fig. 3** XRD patterns of raw MWCNTs, CG, CG-S, CG-S@PANI, PANI, and sublimed sulfur.

**Fig. 4** TGA curves of raw MWCNTs, CG, CG-S, CG-S@PANI, and sublimed sulfur.

**Fig. 5** Nitrogen adsorption-desorption isotherms and DFT pore size distribution curves (inset) of CG, CG-S and CG-S@PANI.

**Fig. 6** Selected charge-discharge profiles of CG-S (a) and CG-S@PANI (b) at 0.02 C for the first three cycles and at 0.2 C for the subsequent cycles.

**Fig. 7** Cyclic stability and Coulombic efficiency of CG-S and CG-S@PANI at 0.2 C.

**Fig. 8** Rate capability of CG-S and CG-S@PANI from 0.05 C to 2 C.

**Fig. 9** Voltage variations of Li/CG-S and Li/CG-S@PANI cells after three discharge/charge cycles at 0.1 C.

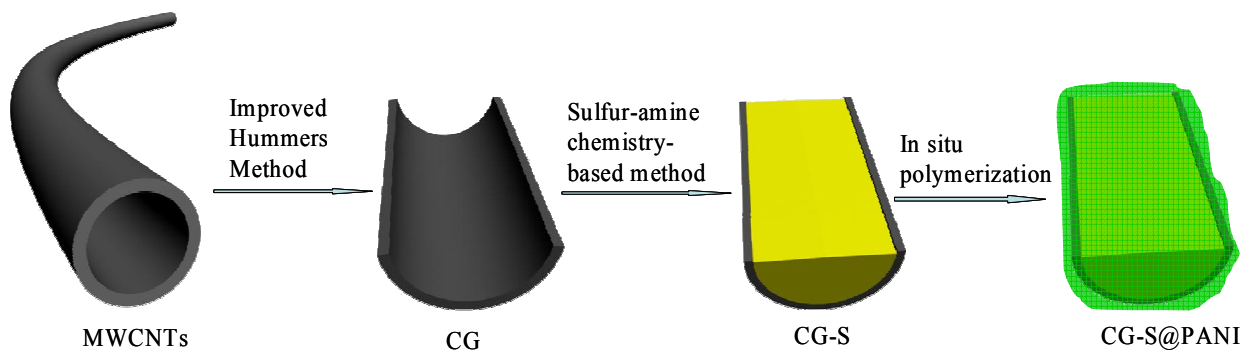
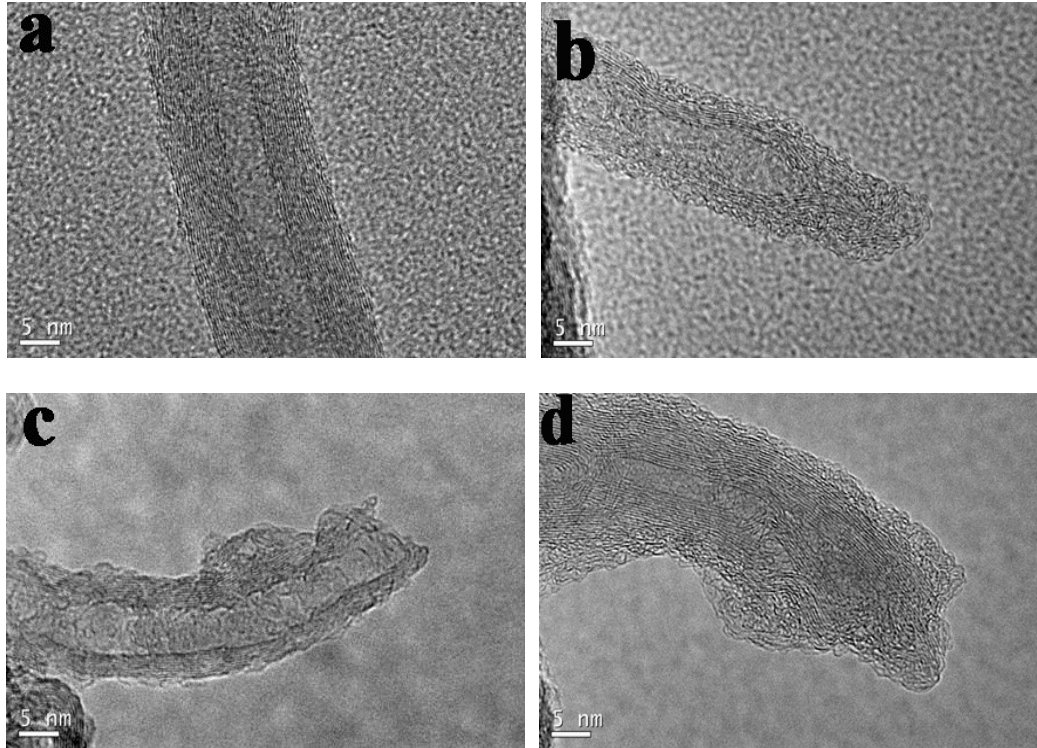


Fig. 1

**Fig. 2**

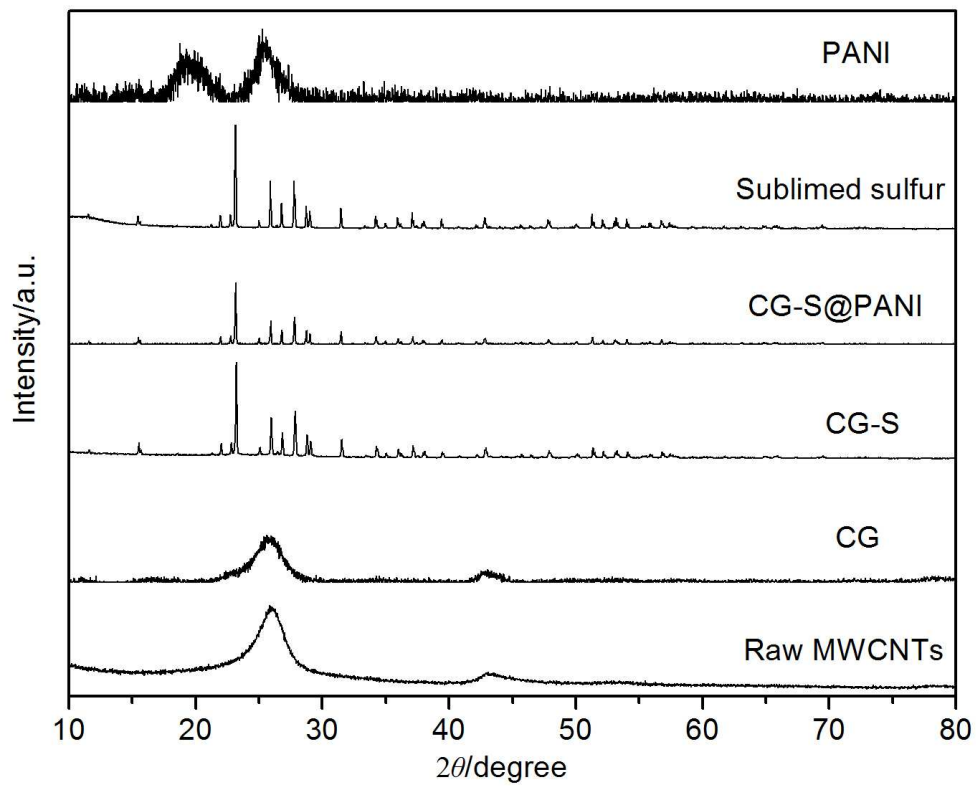


Fig. 3

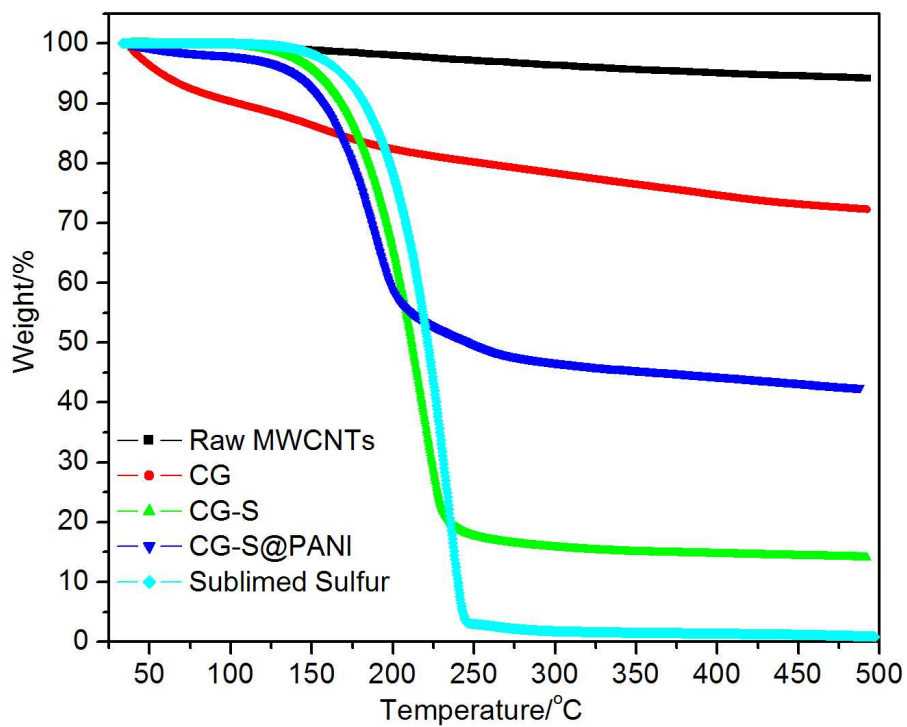


Fig. 4

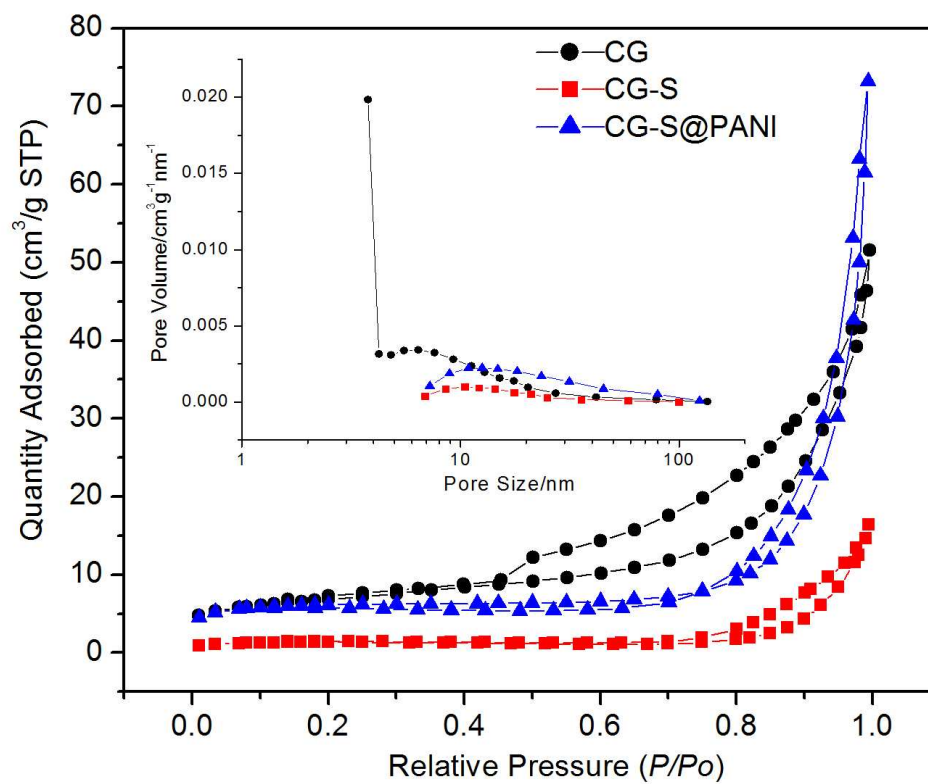


Fig. 5

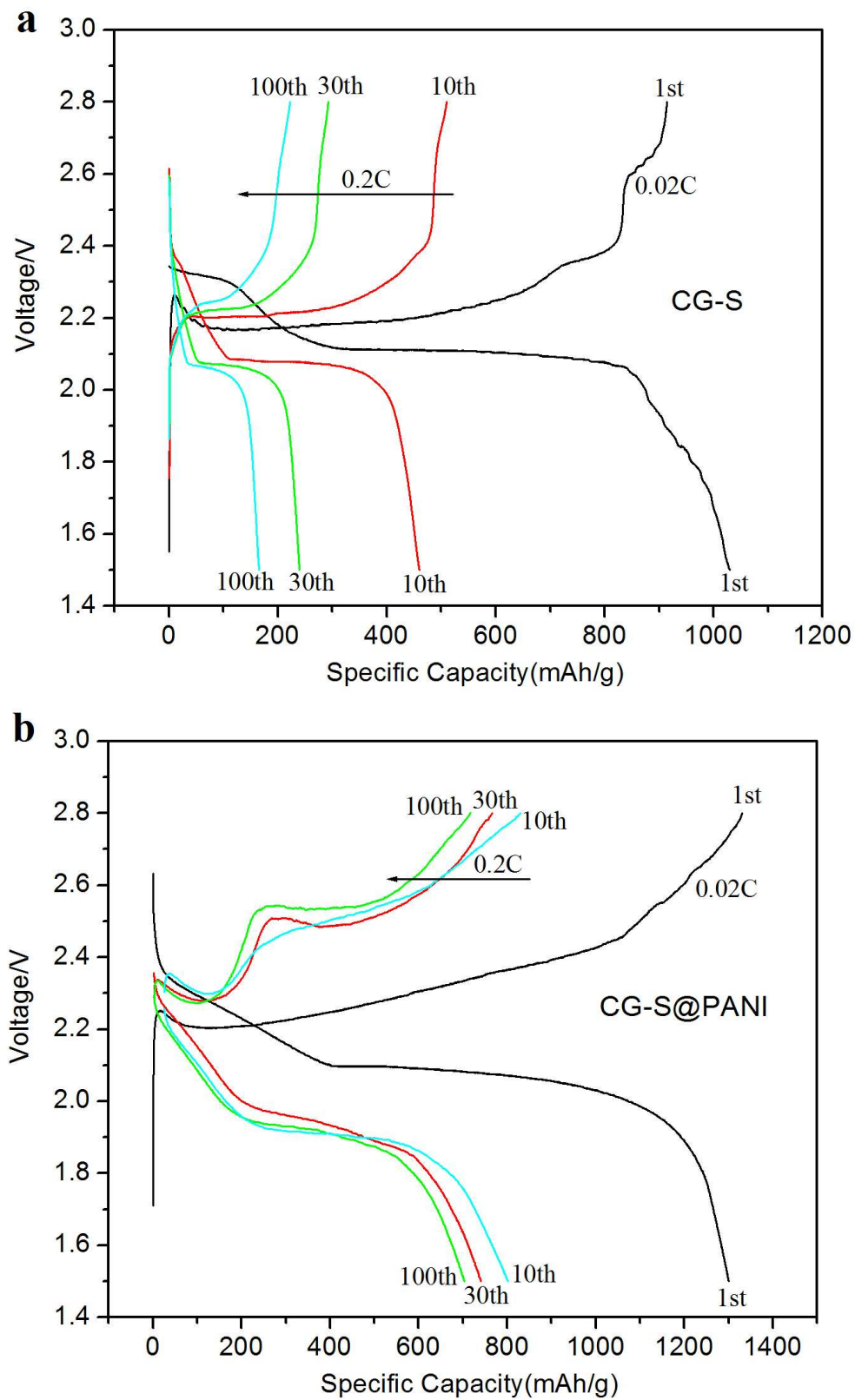


Fig. 6

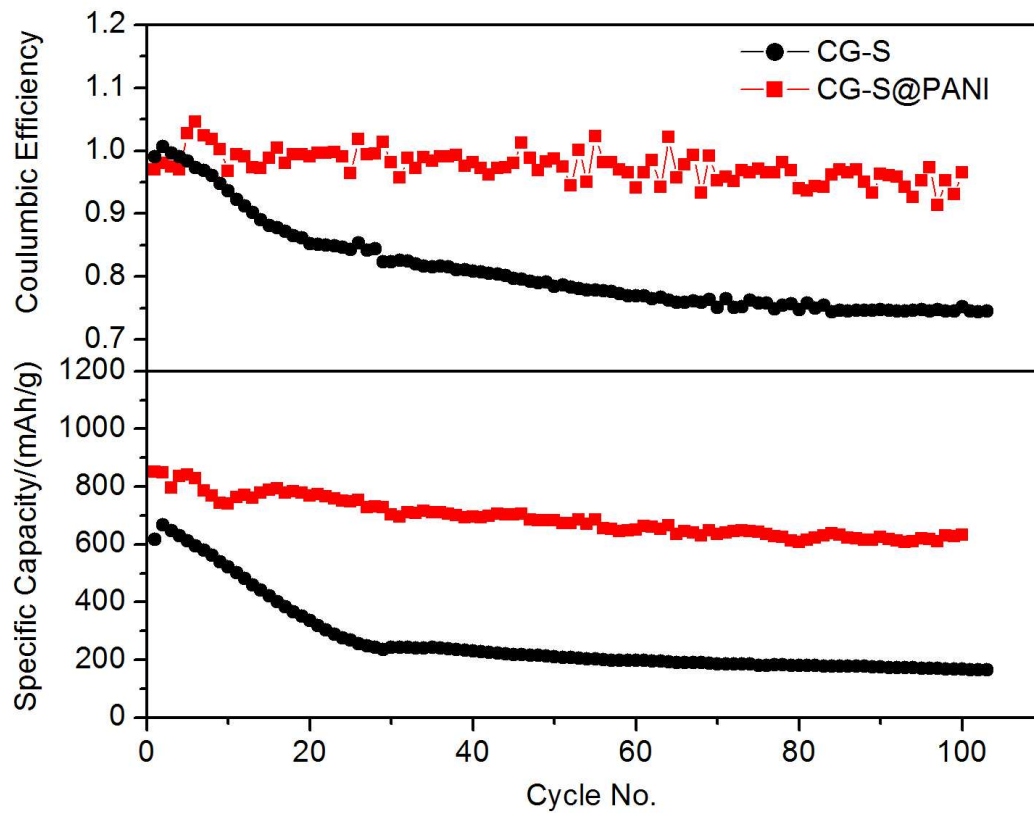


Fig. 7

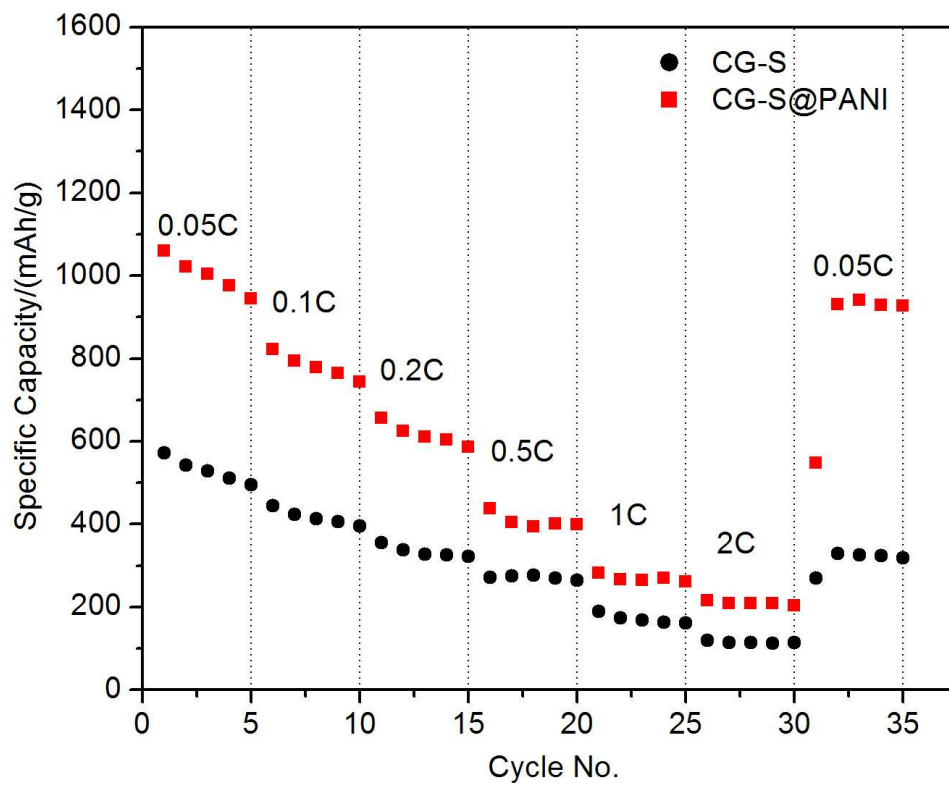
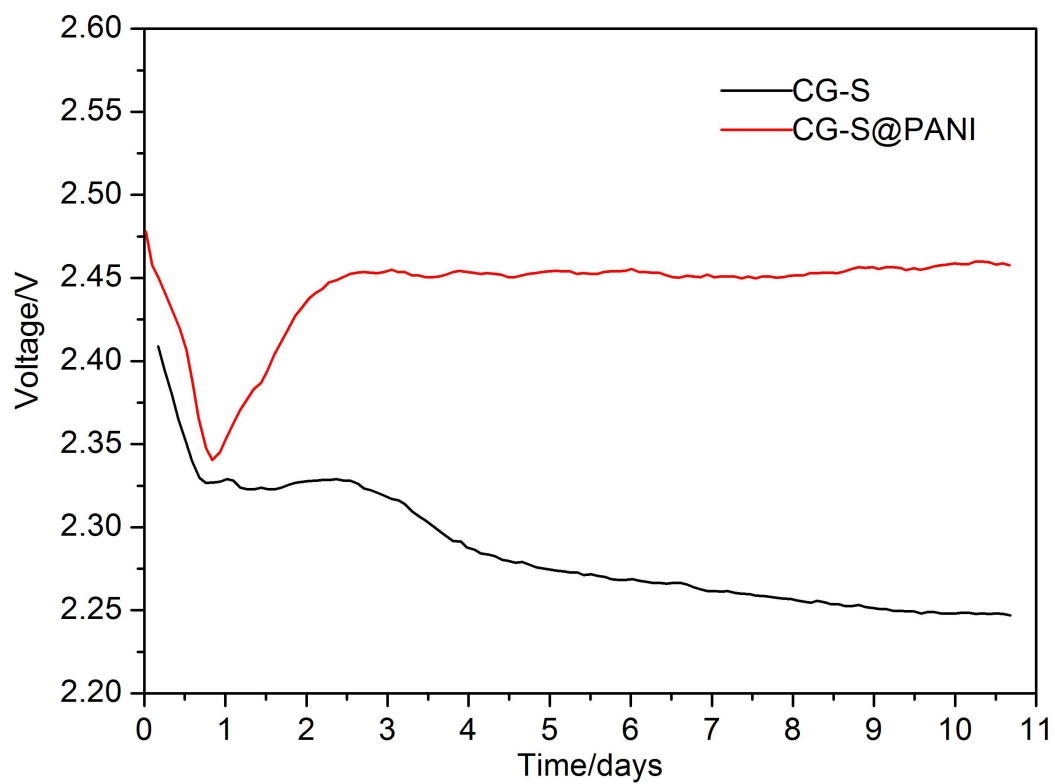
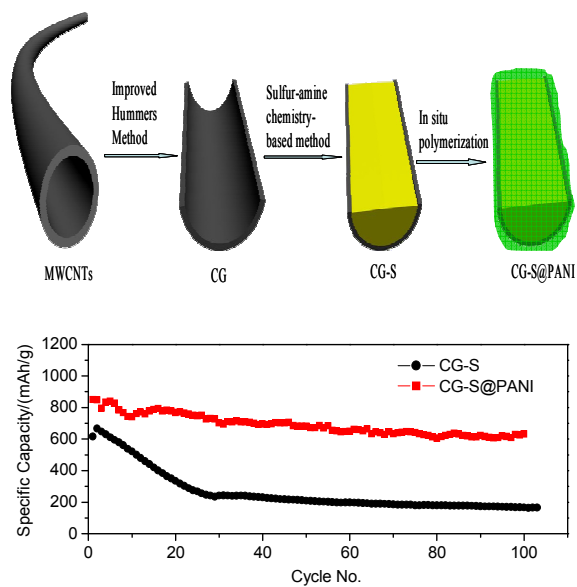


Fig. 8

**Fig. 9**

## Graphical Abstract



CG-S@PANI exhibits good cyclic stability and rate capability due to the co-contribution of CG and PANI.